# Numerical Simulation and Computational Fluid Dynamics Analysis of Two-Dimensional Lid-Driven Cavity Flow Within the Weapon Bay of an Autonomous Fighter Drone

Shabahat Hasnain Qamar, Adrian David Cheok, Miguel Borges Lança, Konstantinos D. Polyzos, Sina Hassanli, and Abdullah Nawab

v1

Sep 4, 2023

https://doi.org/10.32388/8A6RCT

# Numerical Simulation and Computational Fluid Dynamics Analysis of Two-Dimensional Lid-Driven Cavity Flow Within the Weapon Bay of an Autonomous Fighter Drone

Shabahat Hasnain Qamar*[,1], Adrian David Cheok[2], Miguel Borges Lança[3], Konstantinos D. Polyzos[4], Sina Hassanli[5], and Abdullah Nawab[6]

[1] *National University of Science and Technology (NUST), Pakistan*
[2] *iUniversity Tokyo, Japan*
[3] *Instituto Superior Técnico, Lisbon University, Portugal*
[4] *Koenigsegg Automotive AB, Sweden*
[5] *University of Sydney, Australia*
[6] *Institute of Space and Technology (IST), Pakistan*

**Abstract**

The efficient deployment of weapons in military operations is critical for mission success, and the flow of air within the weapon bay of an autonomous fighter drone plays a vital role in achieving this objective. In this paper, we present a comprehensive numerical simulation and computational fluid dynamics (CFD) analysis of the three-dimensional lid-driven cavity flow within the weapon bay of an autonomous fighter drone. To address this challenging problem, we employ CFD analysis and a multigrid approach to solve the Navier-Stokes equations for the aerodynamic problem. Our simulations include high Reynolds numbers of up to 10,000, which demonstrates the potential of CFD analysis in optimizing the design of autonomous fighter drones for military operations. We evaluate the effectiveness of the linked strongly implicit multigrid technique in estimating high-Re fine-mesh flow solutions using the vorticity-stream function formulation of the two-dimensional incompressible Navier-Stokes equations. The model issue is the driven flow in a square cavity, and we consider meshes up to 1024 x 1024 points and combinations with Reynolds numbers as high as 1000. To further improve the accuracy of our simulations, we employ one-dimensional grid clustering coordinate transformations instead of uniform mesh refinement, as the flow field exhibits one or more secondary vortices. Our findings demonstrate that CFD analysis can provide valuable insights into the complex flow dynamics within the weapon bay of autonomous fighter drones, which can lead to the optimization of their design for enhanced mission capabilities. Overall, our study highlights the significance of numerical simulations and CFD analysis in the design and optimization of autonomous fighter drones

* Corresponding author: Shabahat Hasnain Qamar
*E-mail address:* shabahathasnain.q@gmail.com

for military applications. Our results can serve as a basis for future research in the field of UAV aerodynamics and contribute to the development of more efficient and effective military operations.

*Keywords:* Aerial Drones, Robotics, Computational Fluid Dynamics, Unmanned Aerial Vehicles

## *1. Introduction*

Computational fluid dynamics has made significant strides over the past decade, particularly in aerodynamics for both commercial and military applications. One significant application of aerodynamics is the flow of air at high velocity in the missile chamber of fighter jets, where the design of the chamber is critical to ensure that missiles are ready to be deployed as soon as possible [1]. This presents both a challenge and an opportunity for aero designers, especially when dealing with high-speed and high-Reynolds number flows that put a lot of stress on the missile holder. Autonomous Systems (AS), which include robots, fighter drones, fighter planes, self-driving cars, delivery drones, and spray drones, have become increasingly prevalent in military applications [2]. Autonomous drones (UAVs) are capable of executing missions without the need for human intervention, flying to a specific location, selecting their own targets, and carrying out attacks. However, the use of "killer robots" has raised ethical concerns, and while most people may view "autonomous drones" as "smart technology," these drones are actually programmed with a wide range of possible solutions to the many challenges they can encounter while carrying out their duties [3]. If the coupling between the several governing differential equations is not properly respected, either inside the solution domain or at its frontiers, the pace of convergence of the solution might be significantly impacted. Additionally, the rate of convergence is typically highly sensitive to the Reynolds number, mesh size, and overall number of computational points [4].

In recent years, the field of computational fluid dynamics (CFD) has undergone significant advancements, especially in the realm of aerodynamics [5]. One of the most critical applications of aerodynamics is the flow of air in the missile chambers of fighter jet aircraft, which presents both challenges and opportunities for aerodynamic designers [6]. The missile chamber's design is of utmost importance in modern warfare since the missiles must be ready to be deployed as soon as possible. However, the high speed and Reynolds number of the approaching airflow create a significant amount of stress on the missile holder, requiring careful design and optimization [7]. At the same time, there has been a rapid development of autonomous systems (AS) in recent years. These machines are capable of performing desired activities without human intervention and can learn from experience, making them increasingly important in a range of applications, including military operations [8]. Autonomous drones, such as fighter drones, have the ability to fly to a specific location, identify targets, and execute them without human intervention, raising concerns over the use of "killer robots" in warfare. However, autonomous systems have a wide range of potential applications, including the development of drones programmed to operate under different conditions and solve a variety of challenges they may encounter while carrying out their missions [9]. One of the challenges faced in the development of autonomous drones is the need to optimize the flow of air in the missile chamber. The high speed and Reynolds number of the airflow put a lot of stress on the missile holder, requiring careful design and optimization [10]. To address this challenge, computational fluid dynamics (CFD) has become an essential tool in aerodynamic design, providing a means to model and analyze the flow dynamics in the missile chamber. With the help of CFD analysis, aerodynamic designers can optimize the design of the missile chamber for efficient and effective deployment of weapons in military applications [4]. In the field of CFD, the multigrid approach has proven to be a powerful tool for solving aerodynamic problems. While the potential of the multigrid technique has been demonstrated for single differential equations, there are still many issues to be resolved before the technique can be used to solve a system of coupled nonlinear differential equations [11]. The purpose of the current work is to apply the multigrid approach to solve the Navier-Stokes equations for a jet aerodynamic problem, achieving solutions with high Reynolds numbers, high speeds, and mesh refinements. In this study, we present a numerical simulation and computational fluid dynamics (CFD) analysis of three-dimensional lid-driven cavity flow within the weapon bay of an autonomous fighter drone [12]. We apply CFD analysis to model the flow dynamics and use a multigrid approach to solve the Navier-Stokes equations for the aerodynamic problem. The results obtained for the shear-driven flow in the missile chamber in a square cavity at Reynolds numbers as high as 400 and 1000 are then reported, together with the specific details that have to be studied in order to arrive at these answers. We employ two-dimensional grid clustering coordinate transformations instead of uniform mesh refinement since the flow field appears to have one or more secondary vortices. The results of our study demonstrate the potential of CFD analysis and the multigrid approach to optimize the design of autonomous fighter drones for military operations. Our findings have important implications for the development of autonomous systems, including drones and other machines, which must operate under different conditions and perform a wide range of activities without human intervention. In conclusion, we believe that our study provides valuable insights into the use of CFD analysis and the multigrid approach to address the challenges faced in the

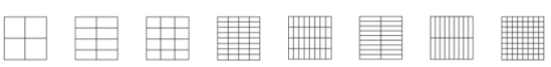

Figure 1. Multiple semi-coarsened grids in 2D with Coarse to Fine Grid

development of autonomous systems for military applications.

### *2. Multigrid Techniques and Structures*

Large systems created by computational fluid dynamics (CFD) call for effective solution techniques. Unsurprisingly, multigrid quickly found uses in CFD. In 1999, the compressible potential equation and shortly after, the incompressible Navier-Stokes equations, were solved using multigrid. Multigrid has developed a tight relationship with CFD over time and is now a component of several important CFD codes [13], [14]. Now that multigrid solutions are available, it is possible to calculate the viscous flow around a whole aircraft configuration. A system of l partial differential equations is used to represent the continuous differential problem under consideration (1).

$$L_j\overline{U}(\bar{x}) = F_j(\bar{x}),\ \ j = 1,2,\dots.,l,\ \ \bar{x}\,\epsilon\, D \tag{1}$$

with the m boundary conditions,

$$B_i\overline{U}(\bar{x}) = G_i(\bar{x}),\ \ i = 1,2,\dots.,m,\ \ \bar{x}\,\epsilon\,\partial D \tag{2}$$

where $x = (x_1, x_2, x_d)$ are the d independent variables of the d-dimensional problem, Fj and Gi are known functions on domain D and its boundary ∂D, respectively, and $L_j$ and $B_i$ are general differential equations. The issue outlined by Eqs. (1) and (2) call for a finite-difference solution in a computational domain with grid spacing h. The linear system of algebraic equations resulting from a chosen difference scheme can be written as, using a superscript h to signify the finite-difference approximation.

$$L_j^h\overline{U^x}(\overline{x^h}) = F_j^h\ (\overline{x^h}) \tag{3}$$

Brandt has calculated the size of the smoothing rate μ, which is the ratio by which each error component is reduced across a Gauss-Seidel relaxation sweep. The smoothing rate of the Fourier components of the error with more slowly increasing wavelengths is relatively poor, it is noticed that Gauss-Seidel relaxation produces a decent smoothing rate for those error components whose wavelength is comparable to the size of the mesh. This feature serves as the cornerstone of the multigrid approach. It understands that a wavelength that is short in relation to a fine mesh is longer in relation to a coarse mesh. Consequently, following the initial two or three iterations on a certain fine mesh. The first step's calculated fine-grid solution must then be adjusted to accurately represent the error's removal of the 2h wavelength content. The multigrid method's fundamental concept is the repeated application of this technique over a series of grids.

Accordingly, the multigrid method makes use of a hierarchy of computational grids Dk with the corresponding grid functions, k = 1, 2..., M. The step size on $D_k$ is h, and $h_k$, and $h_{k+1}$, so that as k decreases, Dk becomes coarser. On the $k^{th}$ grid, Eq. (1) has the discretized approximate form.

$$L_j^k\overline{U^k}(\overline{x^h}) = F_j^k \tag{4}$$

Wesseling [15] referred to this restriction as a "9-point restriction" because it uses that many points, i.e.

$$\left(R_k^{k-1}u^k\right)_{i+1,j+1} = \ \frac{1}{4}u^k_{2i+1,2j+1} \tag{5}$$

The choice of $R_k$ as defined suggests that the prolongation operator $P_i$ also involves nine points so that the value at the cell center is obtained as the arithmetic mean of the four corner points. This leads to the 9-point prolongation operator defined by Wesseling [15] as,

$$\left(\boldsymbol{P_{k-1}^k u^{k-1}}\right)_{\boldsymbol{a}} = \left[\boldsymbol{u_{i+1,j+1}^{k-1} + u_{i+2,j+1}^{k-1} + u_{i+1,j+2}^{k-1}}\right] \tag{6}$$

## *3. Numerical Methodology*

### *3.1 Governing Differential Equations*

ANSYS Fluent for computational fluid dynamics (CFD) permits the simulation of fluid flow and heat transfer phenomena. It models the behaviour of fluid flows using the Navier-Stokes equations, which are the fundamental equations of fluid dynamics. These equations are necessary for an accurate simulation of fluid behaviour because they describe the conservation of mass, momentum, and energy [16]. Additionally, ANSYS Fluent makes use of the Gauss divergence theorem and the Reynolds transport theorem to enable accurate mathematical modelling of complicated fluid events. Numerous fluid flow issues, including turbulent, multiphase, and reactive flows, can be simulated using the software thanks to its sophisticated numerical algorithms and grid generation capabilities [17]. Additionally, it provides support for a number of physical models, including turbulence, heat transfer, and combustion models, allowing the simulation of intricate physical processes.

The momentum conservation equations in the x,y and z directions [18],

$$\begin{aligned}
\rho\left(\frac{\partial u}{\partial t} + u\frac{\partial u}{\partial x} + v\frac{\partial u}{\partial y} + w\frac{\partial u}{\partial z}\right) &= -\frac{\partial p}{\partial x} + \mu\left(\frac{\partial^2 u}{\partial x^2} + \frac{\partial^2 u}{\partial y^2} + \frac{\partial^2 u}{\partial z^2}\right) + \rho g_x \\
\rho\left(\frac{\partial v}{\partial t} + u\frac{\partial v}{\partial x} + v\frac{\partial v}{\partial y} + w\frac{\partial v}{\partial z}\right) &= -\frac{\partial p}{\partial y} + \mu\left(\frac{\partial^2 v}{\partial x^2} + \frac{\partial^2 v}{\partial y^2} + \frac{\partial^2 v}{\partial z^2}\right) + \rho g_y \\
\rho\left(\frac{\partial w}{\partial t} + u\frac{\partial w}{\partial x} + v\frac{\partial w}{\partial y} + w\frac{\partial w}{\partial z}\right) &= -\frac{\partial p}{\partial z} + \mu\left(\frac{\partial^2 w}{\partial x^2} + \frac{\partial^2 w}{\partial y^2} + \frac{\partial^2 w}{\partial z^2}\right) + \rho g_z
\end{aligned} \tag{7}$$

The two-dimensional flow in the cavity can be represented mathematically in terms of the stream function and the vorticity as follows, with the advective terms expressed in conservation form:
Stream Function Equation:

$$\psi_{xx} + \psi_{yy} + \ \omega = 0 \tag{8}$$

Vorticity Transport Equation:

$$\psi_2 \omega\, \omega_{xx} + \omega_{yy} - Re\left[\left(\psi_y \omega\right)_x - \left(\psi_x \omega\right)_y\right] = Re\, \omega_t \qquad (9)$$

The stream function and vorticity are used to express the two-dimensional flow in the cavity mathematically. To capture the complex dynamics of the flow, the stream function equation and the vorticity transfer equation are used. The conservation form of the advective components in these equations ensures an accurate depiction of the fluid flow phenomena. A thorough exploration of the lid-driven cavity flow within the armament bay of an autonomous fighter drone is made possible by these mathematical formulations, which offer a formal foundation for carrying out numerical simulations and computational fluid dynamics analyses. To evaluate the flow behaviour inside a certain grid arrangement, a thorough computational fluid dynamics (CFD) analysis was carried out. The importation of the grid, which served as the computing environment for the flow solver issue, is shown in Figure 2. The density and viscosity of the fluid, among other fluid parameters, were precisely specified to reflect the behaviour of the fluid under investigation. The governing equations were discretized using a suitable discretization scheme, as shown in Figure 3, ensuring accurate and effective numerical calculations. By establishing suitable boundary conditions, taking into account inlet, exit, and wall conditions, real-world situations were replicated. Convergence monitors were built to track the convergence of the numerical solution. The simulations were then run to address the flow issue, and thorough findings were produced. The flow behaviour of these results was then thoroughly analyzed in order to derive insightful conclusions. As shown in Figure 3, the combined outcomes of the grid import and flow solver issue design considerably aided in the thorough analysis of the flow behaviour.

*3.2 Boundary Conditions*

In fluid dynamics, it is well-established that the zero-slip requirement for nonporous walls leads to the vanishing of w and its normal derivatives at all boundaries. However, this does not provide a direct condition for the tangential velocity component, o, at the walls, as is widely recognized in the field. This poses a challenge in the numerical solution of the Navier-Stokes equations, as a consistent treatment of boundary conditions is essential for accurate and reliable results [19]. One possible approach to overcome this challenge is to solve the equations for u and v simultaneously and apply all boundary conditions implicitly. This method has shown promising results in certain scenarios, but it may not be sufficient for all cases. Further research is needed to explore alternative techniques that can effectively address the boundary condition issue in numerical simulations of fluid dynamics. Ultimately, the development of robust and efficient computational methods will enable more accurate predictions of complex fluid flows and enhance our understanding of fundamental physical phenomena [10].

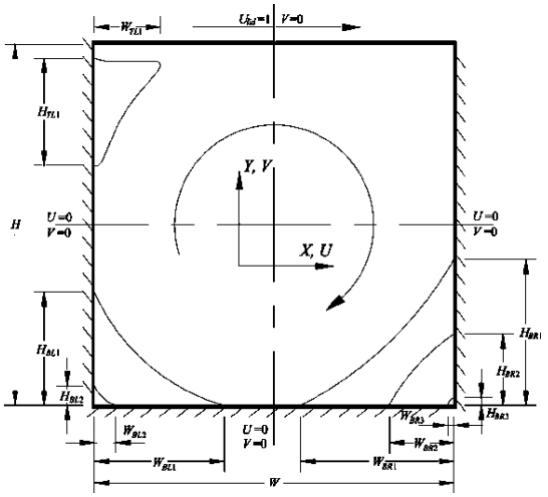


Figure 2. Expressions for vorticity at other boundaries

The cavity flow structure, along with the related coordinates, nomenclature, and boundary conditions, are shown in the accompanying diagram (Fig 4). In the high-tech research report, the experimental setup or computing domain is represented visually by this figure. The term "cavity flow configuration" describes a particular pattern of fluid flow that takes place inside an enclosed space called a cavity. Depending on the experimental or computational setup, the cavity in this scenario could have any shape, including a square, rectangle, or an irregular shape. The research report is particularly interested in the fluid movement inside the hollow. Defining the spatial location of distinct places within the cavity requires the use of coordinates. The x-axis and the y-axis in the illustration represent the coordinate system in a typical way. These axes give researchers the ability to pinpoint precise locations inside the hollow and gauge lengths or widths. Axes should be scaled and measured in exact accordance with the standards used in the study report. The labelling or naming of various elements, factors, or parameters inside the cavity flow configuration is referred to as nomenclature. There may be comments or labels on the graphic designating certain areas, flow variables, or physical quantities pertinent to the study. These labels are essential for clearly conveying the details to readers and assuring their understanding. The behaviour of the fluid flow near the cavity's edges or borders is defined by boundary conditions. The picture depicts the precise boundary conditions that were enforced throughout the research investigation. These requirements could be velocity profiles, pressure gradients, temperature distributions, or any other pertinent restrictions. To accurately simulate or analyse the fluid flow behaviour inside the hollow, certain conditions are necessary.

*3.3 Discretization*

The numerical error (E) can be defined as the difference

between the exact analytical solution (Φ) of a variable of interest and its numerical solution ($\phi$), i.e.,

$$E(\phi) = \Phi - \phi \quad (10)$$

In the context of numerical methods for solving partial differential equations, the choice of mesh or grid on which the equations are discretized can have a significant impact on the accuracy and efficiency of the solution. In many cases, a uniform mesh may be sufficient for obtaining a reasonable approximation to the solution. However, in situations where the solution exhibits localized features or sharp gradients, a non-uniform mesh may be necessary to capture these details accurately [20]. One approach to handling non-uniform meshes is to use grid-clustering coordinate transformations. This involves mapping the physical domain to a transformed computational domain where the mesh is uniform, and then applying a clustering transformation to obtain a non-uniform mesh in the physical domain. While effective, this approach can be computationally expensive and may introduce additional errors in the solution [21]. An alternative approach is to use a multigrid solution technique, which can handle local mesh refinement without the need for coordinate transformations. In this method, progressively finer grids are constructed in designated subdomains of the computational space, allowing for local refinement where necessary. This can lead to significant improvements in both the accuracy and efficiency of the solution, particularly in cases where the solution exhibits localized features or sharp gradients [22], [23]. All second-order derivatives in Eqs. (12) are approximated by second-order accurate central finite-difference methods. According to a formal suggestion made by Khosla and Rubin [24], the convective terms in Eq. (11) are represented by a first-order accurate upwind difference scheme that includes its second-order accurate term as a postponed correction [25]. In theory [18], [26], it is expected that $p_E$ (effective order) and $p_U$ (apparent order) $\rightarrow p_L$ for $h \rightarrow 0$. In other words, it is expected that the practical orders ($p_E$ and $p_U$), which are calculated with the numerical solution of this work u solutions of each variable of interest, tend toward the asymptotic order ($p_L$), foreseen a priori, when the size of the control volumes (h) tends toward zero. The effective order ($p_E$) of the true error is defined by [18],

$$p_E = log[E(\phi_2)/E(\phi_1)] \quad (11)$$

where $E(\phi 1)$ and $E(\phi 2)$ are true discretization errors of the numerical solutions $\phi 1$ and $\phi 2$ obtained, respectively, with fine (h1 ) and coarse (h2) grids; h = size of the control volumes (in this work, $h = \Delta x = \Delta y$); and r = h2 /h1 (grid refinement ratio). According to Eq. (12), the effective order ($p_E$) is a function of the true discretization error of a variable of interest. Thus, for problems for which an analytical solution is known, it can be used to verify a posteriori if, as $h \rightarrow 0$, one obtains $p_L$. When E is unknown, ($p_E$) cannot be calculated. In this case, one can use the concept of observed or apparent order ($p_U$) defined by [27][28],

$$p_U = log(\phi_2 - \phi_3)/(\phi_1 - \phi_2) \quad (12)$$

where $\phi 1$, $\phi 2$ and $\phi 3$ = numerical solutions obtained, respectively, with fine ($h_1$), coarse ($h_2$) and super coarse ($h_3$) grids, and $r = h_3/h_2 = h_2/h_1$. Several studies [13], [14], [29]–[31] achieved excellent results when employing multiple Richardson extrapolations (MRE) to reduce the discretization error of $\psi_{min.}$ These authors, however, only applied this procedure to the finest of four grids, yielding up to three

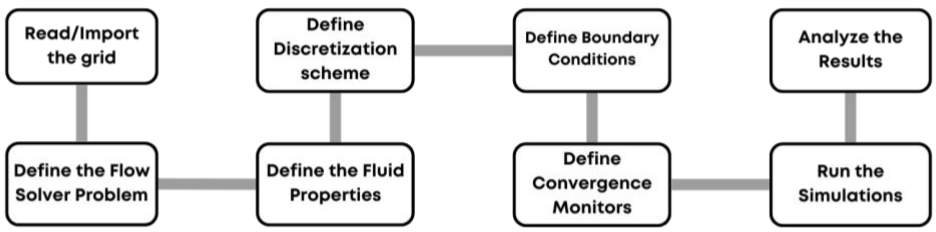


Figure 4. Workflow for Computational Fluid Dynamics (CFD) study

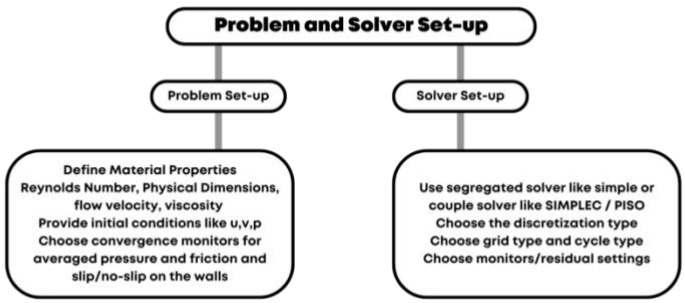


Figure 4. Workflow for Computational Fluid Dynamics (CFD) study

extrapolations. In the current study, this method was applied to practically all variables of interest with up to ten grids, producing up to nine extrapolations for the best grid employed (1024 x 1024). Using,

$$\phi_{1,m_\infty} = \phi_{1,(m-1)_\infty} + \frac{\phi_{1,(m-1)_\infty} - \phi_{2,(m-1)_\infty}}{r^{pv(m)}-1} \quad (12)$$

where $\phi_{1,m\infty}$ is the numerical solution of the variable of interest ($\phi$) with m extrapolations on the fine grid ($h_1$ ); $\phi_{1,(m-1)\infty}$ and $\phi_{2,(m-1)\infty}$ are numerical solutions with (m-1) extrapolations on the fine ($h_1$ ) and coarse ($h_2$ ) grids; $r = h_2 / h_1$ (grid refinement ratio); m = number of Richardson extrapolations, with m = 0 being the numerical solution obtained in grid h without any extrapolation. Different grids with numerical solutions of $\phi$ without any extrapolation; $p_V(m)$ = true orders [32]–[34] of the discretization error, with $p_V(1) = p_L$. For the numerical model used in this work, $p_V = 2$, 4, 6 ... for all variables of interest, except for x and y coordinates of $\psi_{min}$, $u_{min}$, $v_{min}$ and $v_{max}$, of which values of $p_V$ are unknown. In practical situations, a numerical solution is obtained because the analytical solution is unknown. Hence, the true value of the numerical error is also unknown. Therefore, the numerical error must be estimated. The estimated discretization error (U) of $\phi_{1,\,(nm-1)\infty,}$ i.e., of the numerical solution with the highest possible number of extrapolations in the finest grid, will be considered equal to,

$$U(\phi_{1,(nm-1)_\infty}) = |\phi_{1,(nm-2)_\infty} - \phi_{2,(nm-2)_\infty}| \quad (13)$$

which is the module of the difference with the highest number of extrapolations that can be calculated between the two finest grids. In the case of the x and y coordinates of $\psi_{min}$, $u_{min}$, $v_{min}$ and $v_{max}$,

$$U(x,y) = |\phi_{1024x1024} - \phi_{512x512}| \quad (14)$$

where $\phi_{1024x1024}$ and $\phi_{512x512}$ are the numerical solutions obtained without extrapolation on 1024 x 1024 and 512 x 512 nodes grids. The resulting algebraic equations are guaranteed to have diagonal dominance, which gives the evolving solutions the requisite stability quality while regaining second-order accuracy at convergence.

### *3.4 Multigrid Procedure*

Instead of using a corrective strategy, the full approximation scheme (FAS) was used for the current nonlinear situation. Additionally, the CSI process employed for relaxation typically yields a convergent coarse-grid solution, hence the full multigrid (FMG) algorithm was chosen over the cycle algorithm. The cycling algorithm might also be employed for the higher-Re cases computed, with the answer of an earlier calculation with a lower value of Re serving as the first approximation of the finest-grid solution [34]–[38]. Finally, the "accommodative" form of the multigrid approach was employed to manage the computational process by monitoring convergence as well as convergence rate during the process of relaxing on a particular grid [39]. There is a variant of the classical problem of which an analytical solution is known and is given by [40], [41]. The analytical solution of u and v is,

$$u(x,y) = 8(x^4 - 2x^3 + x^2)(4y^3 - 2y) \quad (15)$$

$$v(x,y) = -8(4x^3 - 6x^2 + 2x)(y^4 - y^2) \quad (16)$$

All numerical solutions in this work were obtained with ten different grids: 2 x 2, 4 x 4, 8 x 8 and so on up to 1024 x 1024 real control volumes. All simulations of this study were made in a Dell G4 12-Gen Intel i9-12900H 5 GHz Turbo 16 GB DDR5 with NVIDIA® GeForce RTX™ 3070 Ti, 8 GB GDDR6 with 1024 x 1024 nodes grid.

## *4. Results*

In the classical problem [23], [32], [35], [42]–[44] of laminar flow inside a square cavity, the lid velocity ($U_T$) is constant and has a unitary value. The other boundary conditions are shown in Fig. 1. At lid corners, u = 0 on one side and u = 1 on the other. The Reynolds number (Re) is defined by,

$$Re = \rho U_T \frac{L}{\mu} \quad (17)$$

where L = 1 m, dimension of the side of the square cavity; ρ = 1 kg/m3, density; and μ is the viscosity in Pa.s, obtained from Eq. (19) for a given Re. Numerical solutions were obtained for Re = 0.01, 10, 100, 400 and 1000. The initial estimate used was u = v = p = 0. The following maximum values were produced by the stream function value (psi) in y = 1, which ought to be null for each of the 1024 control volumes at the cavity lid: For Re = 0.01, 10, 100, 400, and 1000, the corresponding values are $5.9 \times 10^{-16}$, $1.7 \times 10^{-15}$, $5.4 \times 10^{-16}$, $1.0 \times 10^{-15}$, and $2.3 \times 10^{-15}$. These numbers, which are at the level of double precision used in this work, are quite near to the null one.

Figure 4 displays the velocity profiles in the two directions at the cavity centre. The numerical solution of this work utilising the 1024 x 1024 grid is extremely consistent with the numerical solutions of [20], [30], [23], [26], [35], [42]–[46] The streamline patterns seen in the cavity flow are represented by the contours of the vorticity in Fig 6 and Fig 7. concentrated vorticity contours show the formation of numerous high-vorticity gradient zones as the Reynolds number (Re) rises. It's interesting to note that these areas don't line up with the cavity's physical borders. In the current study, we used uniform mesh refinement to accurately represent these complicated flow phenomena. Alternative strategies should be taken into account, such as using a modified non-Cartesian coordinate system or a solution-adaptive local mesh refining method. The vorticity near the middle of the moving wall or the minimum value of vorticity, In the cavity, boundary is an often compared quantity for cavity flows. It is commonly known that at Re = 100, the primary vortex's centre is first displaced towards the upper right corner. The main vortex eventually travels in the direction of the cavity's geometric centre as Re rises. It's interesting to note that for Re > 5000, the major vortex's location nearly becomes invariant.

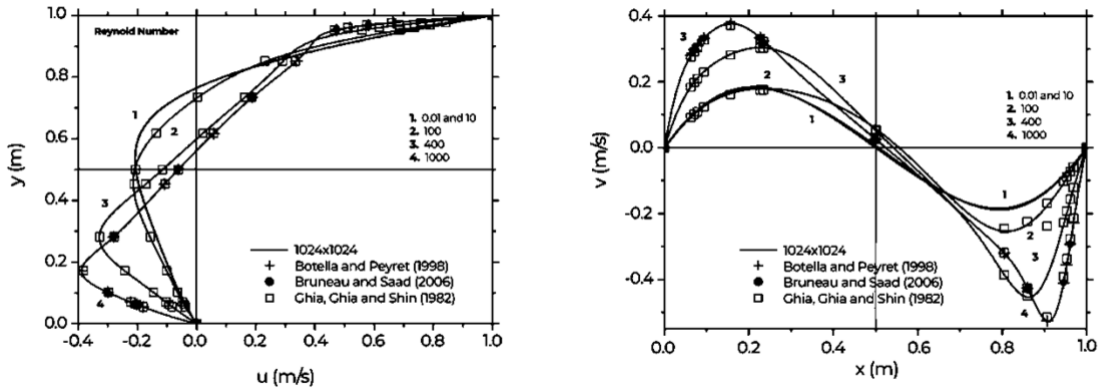


Figure 5. u at x = ½ and v at y = ½ for the classical problems

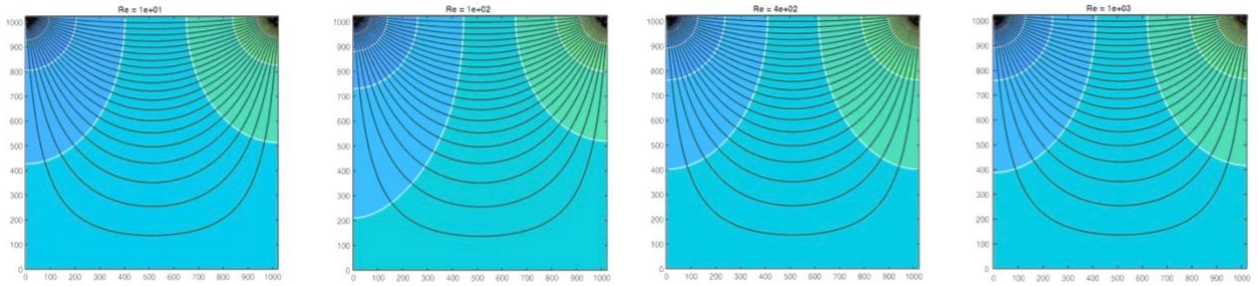


Figure 6. Contour Pattern of solution when Mesh 1024 X 1024 and Re=10, 100, 400, and 1000

For secondary vortices, they first manifest themselves close to the corners (or close to the wall for the vortex TL). The centres of these secondary vortices gradually gravitate towards the cavity's centre as Re increases. Notably, for greater levels of Re, the secondary eddies' convection becomes visible as shown by the direction in which their centres travel. This sentence justifies the observations stated in the study article in Figure 6 and offers an explanation. The development of strong vorticity gradients, the misalignment of vorticity regions with geometric boundaries, the consideration of uniform mesh refinement, the investigation of alternative coordinate systems and mesh refinement methods, and the behaviour of primary and secondary vortices with different Reynolds numbers are all highlighted.

### *5. Conclusion*

In conclusion, this research study aimed to generate fine-mesh solutions for the lid-driven cavity problem with a Reynolds number (Re) up to 1000 with the objective of assessing the accuracy and efficacy of the analysis, as well as the efficiency of the computer programs. The convergence requirement was used to quantify the relative change between iterations and functioned as a precision indicator for the computational method. The velocity profiles derived from the CFD simulations showed strong agreement with the validated data, confirming the accuracy of the simulation results. The two-dimensional flow field and variations in drag coefficients around vertical cylinders were examined using the SIMPLE model and the ANSYS Pressure-based Solver. Notably, vortex shedding, and the wake flow were considerably influenced by the shape of the cylinders. It was also noted that using a triangular mesh yielded slightly different results from using a quad mesh, indicating the need for additional research into the influence of mesh types on simulation outcomes. Despite shedding light on certain crucial features of the lid-driven cavity problem, complicated flow systems still have more mysteries to be solved. Future studies should concentrate on pinpointing and comprehending the precise unknowns and complexities connected to such systems in order to facilitate more thorough and precise modelling. Additionally, the development of unmanned aerial vehicles (UAVs) has completely changed a number of industries thanks to their cutting-edge hardware, which includes physical models, Ground Control Stations (GCS), modern sensors, and improved communication systems. UAVs have a wide variety of uses, including search and rescue, climate monitoring, surveillance, weather forecasting, and mapping. These uses span both military and civilian missions. The strength of the internet and these technical breakthroughs have revolutionized emergency evacuations during natural catastrophes like storms, floods, and bushfires. However, it is crucial to address problems and issues including legal

frameworks, privacy concerns, and safety precautions that may come up with the increased use of UAVs. We can fully utilise the capabilities of UAVs and progress their use by proactively resolving these problems. Overall, this research study demonstrates the accuracy of CFD models and offers helpful insights into the lid-driven cavity problem. Additionally, it highlights how UAVs are transforming numerous businesses and demonstrates how they have the potential to disrupt a number of other fields, including emergency response. The future of fluid dynamics and UAV technology looks bright with continuing research and development, opening doors to new opportunities and breakthroughs yet to be discovered.

### *6. Conflict of Interest*

The authors declare that they have no conflict of interest with respect to this research study. They have not received any financial or non-financial benefits or support that may have influenced the design, execution, or reporting of this research. Additionally, they have no personal, professional, or academic affiliations that could be perceived as having a potential influence on this study.


### *7. Funding*

This research was conducted without any external funding. The authors solely bear the responsibility for the study design, data collection, analysis, interpretation, and manuscript preparation.


### *8. Ethical Approval*

Ethical approval was not required for this study, as it does not involve any studies of human participants or animals performed by any of the authors.


### *10. Acknowledgements*

We would like to express our sincere gratitude to the Department of Mechanical Engineering at the National University of Science and Technology (NUST) and the Quantum Commutating Lab (NUST) for their support in this research by providing computational facilities. We are grateful to Dr. Imran Akhtar PhD. for his valuable insights and assistance with the Computational Fluid Dynamics (CFD) simulations, Muhammad Moazzam Ali from the University of Engineering and Technology (UET), Taxila and Hasnain Zia from the National University of Science and Technology (NUST) their expertise and guidance were instrumental in the success of this study.


## Reference


[1] K. (Kimon) Valavanis, “Advances in unmanned aerial vehicles : state of the art and the road to autonomy,” p. 543, 2007.

[2] A. North, R. Siegwart, and W. Engel, “Autonomous Solar UAV for Sustainable Flights,” Advances in Unmanned Aerial Vehicles, pp. 377–405, Feb. 2008, doi: 10.1007/978-1-4020-6114-1_12.

[3] B. Ludington, E. N. Johnson, and G. J. Vachtsevanos, “Vision Based Navigation and Target Tracking for Unmanned Aerial Vehicles,” Advances in Unmanned Aerial Vehicles, pp. 245–266, Feb. 2008, doi: 10.1007/978-1-4020-6114-1_8.

[4] P. Wesseling and C. W. Oosterlee, “Geometric multigrid with applications to computational fluid dynamics,” J Comput Appl Math, vol. 128, no. 1–2, pp. 311–334, Mar. 2001, doi: 10.1016/S0377-0427(00)00517-3.

[5] A. Bhuvaneswari, V. K. Chandrasekar, M. Senthilvelan, and M. Lakshmanan, “On the complete integrability of a nonlinear oscillator from group theoretical perspective,” J Math Phys, vol. 53, no. 7, Jul. 2012, doi: 10.1063/1.4731238.

[6] M. Holubčík, G. Koman, and W. Sroka, “MANAGING THE DEPLOYMENT OF UAV SYSTEMS IN SLOVAKIA,” Polish Journal of Management Studies, vol. 26, no. 2, pp. 172–188, Dec. 2022, doi: 10.17512/PJMS.2022.26.2.11.

[7] R. C. Arkin, “The case for ethical autonomy in unmanned systems,” Journal of Military Ethics, vol. 9, no. 4, pp. 332–341, Dec. 2010, doi: 10.1080/15027570.2010.536402.

[8] K. Puchała, G. Moneta, E. Szymczyk, and V. Hutsaylyuk, “The Concept and Preliminary Design of a New Drone Destined for Military Rescue/Medical Missions,” Challenges to National Defence in Contemporary Geopolitical Situation, vol. 2022, no. 1, pp. 248–253, Oct. 2022, doi: 10.47459/CNDCGS.2022.32.

[9] A. Konert and T. Balcerzak, “Military autonomous drones (UAVs) - from fantasy to reality. Legal and Ethical implications.,” Transportation Research Procedia, vol. 59, pp. 292–299, Jan. 2021, doi: 10.1016/J.TRPRO.2021.11.121.

[10] J. de Gier, J. Bergmans, and H. Hildmann, “Hierarchical Plan Execution for Cooperative UxV Missions,” Robotics, vol. 12, no. 1, Feb. 2023, doi: 10.3390/ROBOTICS12010024.

[11] S. Thabet and T. H. Thabit, “Computational Fluid Dynamics: Science of the Future,” International Journal of Research and Engineering, vol. 5, no. 6, pp. 430–433, 2018, doi: 10.21276/IJRE.2018.5.6.2.

[12] A. Sheeba, P. Mathew, and P. M. Jose, “Numerical investigations on the heat transfer characteristics of tube in tube helical coil heat exchanger,” J Phys Conf Ser, vol. 1355, no. 1, Nov. 2019, doi: 10.1088/1742-6596/1355/1/012005.

[13] M. M. Butt and Y. Yuan, “A Full Multigrid Method for Distributed Control Problems Constrained by Stokes Equations,” Numerical Mathematics, vol. 10, no. 3, pp. 639–

655, Aug. 2017, doi: 10.4208/NMTMA.2017.M1637.
[14] M. M. Butt and A. Borzì, “Formulation and multigrid solution of Cauchy-Riemann optimal control problems,” Comput Vis Sci, vol. 14, no. 2, pp. 79–90, Feb. 2011, doi: 10.1007/S00791-011-0161-9.
[15] P. Wesseling, “Principles of Computational Fluid Dynamics,” vol. 29, 2001, doi: 10.1007/978-3-642-05146.
[16] J. Keogh, G. Doig, T. J. Barber, and S. Diasinos, “The Aerodynamics of a Cornering Inverted Wing in Ground Effect,” Applied Mechanics and Materials, vol. 553, pp. 205–210, 2014, doi: 10.4028/www.scientific.net/amm.553.205.
[17] R. L.S., C. J., F. M.V., and K. K., “Investigation of forcing boundary layer transition on a single-element inverted wing in ground effect,” The International Vehicle Aerodynamics Conference. Elsevier, pp. 199–211, 2014. doi: 10.1533/9780081002452.6.199.
[18] C. H. Marchi, R. Suero, and L. K. Araki, “The lid-driven square cavity flow: numerical solution with a 1024 x 1024 grid,” Journal of the Brazilian Society of Mechanical Sciences and Engineering, vol. 31, no. 3, pp. 186–198, 2009, doi: 10.1590/S1678-58782009000300004.
[19] M. R. Ahmed and S. D. Sharma, “An Investigation on the Aerodynamics of a Symmetrical Airfoil in Ground Effect,” Exp Therm Fluid Sci, vol. 29, no. 6, pp. 633–647, Jul. 2005, doi: 10.1016/j.expthermflusci.2004.09.001.
[20] C. Y. Wu, R. Girshick, K. He, C. Feichtenhofer, and P. Krähenbühl, “A Multigrid Method for Efficiently Training Video Models,” Proceedings of the IEEE Computer Society Conference on Computer Vision and Pattern Recognition, pp. 150–159, Dec. 2019, doi: 10.1109/CVPR42600.2020.00023.
[21] F. Lv, X. Zhang, C. Ji, and Z. Rao, “Theoretical and experimental investigation on local turbulence effect on mixed-lubrication journal bearing during speeding up,” Physics of Fluids, vol. 34, no. 11, Nov. 2022, doi: 10.1063/5.0122039.
[22] A. Brandt and O. E. Livne, “Multigrid Techniques,” Multigrid Techniques, Jan. 2011, doi: 10.1137/1.9781611970753.
[23] Y. Cao, Z. Chen, and M. Gunzburger, “Error analysis of finite element approximations of the stochastic Stokes equations,” Adv Comput Math, vol. 33, no. 2, pp. 215–230, Aug. 2010, doi: 10.1007/S10444-009-9127-6.
[24] S. G. Rubin and P. K. Khosla, “Polynomial interpolation methods for viscous flow calculations,” J Comput Phys, vol. 24, no. 3, pp. 217–244, Jul. 1977, doi: 10.1016/0021-9991(77)90036-5.
[25] Z. Zaheer, K. E. Reby Roy, G. S. Nair, V. Ragipathi, and U. V. Niranjan, “CFD analysis of the performance of different airfoils in ground effect,” J Phys Conf Ser, vol. 1355, no. 1, p. 012006, Nov. 2019, doi: 10.1088/1742-6596/1355/1/012006.
[26] M. D. Gunzburger, H. C. Lee, and J. Lee, “Error estimates of stochastic optimal Neumann boundary control problems,” SIAM J Numer Anal, vol. 49, no. 4, pp. 1532–1552, 2011, doi: 10.1137/100801731.
[27] G. De Vahl Davis, “Natural convection of air in a square cavity: A bench mark numerical solution,” Int J Numer Methods Fluids, vol. 3, no. 3, pp. 249–264, May 1983, doi: 10.1002/FLD.1650030305.
[28] C. H. Marchi and A. F. Carvalho da Silva, “UNIDIMENSIONAL NUMERICAL SOLUTION ERROR ESTIMATION FOR CONVERGENT APPARENT ORDER,” http://dx.doi.org/10.1080/10407790190053888, vol. 42, no. 2, pp. 167–188, Aug. 2010, doi: 10.1080/10407790190053888.
[29] E. Erturk, T. C. Corke, and C. Gökçöl, “Numerical solutions of 2-D steady incompressible driven cavity flow at high Reynolds numbers,” Int J Numer Methods Fluids, vol. 48, no. 7, pp. 747–774, Jul. 2005, doi: 10.1002/FLD.953.
[30] M. M. Butt, “Multigrid Method for Optimal Control Problem Constrained by Stochastic Stokes Equations with Noise,” Mathematics 2021, Vol. 9, Page 738, vol. 9, no. 7, p. 738, Mar. 2021, doi: 10.3390/MATH9070738.
[31] P. Chen, A. Quarteroni, and G. Rozza, “Multilevel and weighted reduced basis method for stochastic optimal control problems constrained by Stokes equations,” Numer Math (Heidelb), vol. 133, no. 1, pp. 67–102, May 2016, doi: 10.1007/S00211-015-0743-4.
[32] C. H. Marchi and A. F. Carvalho da Silva, “UNIDIMENSIONAL NUMERICAL SOLUTION ERROR ESTIMATION FOR CONVERGENT APPARENT ORDER,” http://dx.doi.org/10.1080/10407790190053888, vol. 42, no. 2, pp. 167–188, Aug. 2010, doi: 10.1080/10407790190053888.
[33] H. C. Lee and M. D. Gunzburger, “Comparison of approaches for random PDE optimization problems based on different matching functionals,” Computers and Mathematics with Applications, vol. 73, no. 8, pp. 1657–1672, Apr. 2017, doi: 10.1016/J.CAMWA.2017.02.002.
[34] I. Babuška, R. Tempone, and G. E. Zouraris, “Solving elliptic boundary value problems with uncertain coefficients by the finite element method: The stochastic formulation,” Comput Methods Appl Mech Eng, vol. 194, no. 12–16, pp. 1251–1294, Apr. 2005, doi: 10.1016/J.CMA.2004.02.026.
[35] C. Feng, S. Shu, J. Xu, and C. S. Zhang, “Numerical study of geometric multigrid methods on CPU-GPU heterogeneous computers,” Adv Appl Math Mech, vol. 6, no. 1, pp. 1–23, 2014, doi: 10.4208/AAMM.2013.M87.
[36] M. M. Butt, “A multigrid solver for Stokes control problems,” Int J Comput Math, vol. 94, no. 12, pp. 2297–2314, Dec. 2017, doi: 10.1080/00207160.2017.1283022.

[37] T. Rees and A. J. Wathen, “Preconditioning iterative methods for the optimal control of the Stokes equations,” SIAM Journal on Scientific Computing, vol. 33, no. 5, pp. 2903–2926, 2011, doi: 10.1137/100798491.
[38] C. W. Oosterlee and F. J. G. Lorenz, “Multigrid methods for the Stokes system,” Comput Sci Eng, vol. 8, no. 6, pp. 34–43, Nov. 2006, doi: 10.1109/MCSE.2006.115.
[39] M. Mohebbi and M. A. Rezvani, “Numerical analysis of aerodynamic performance of regional passenger train under crosswind conditions,” International Journal of Vehicle Structures and Systems, vol. 5, no. 2, pp. 68–74, 2013, doi: 10.4273/IJVSS.5.2.05.
[40] L. S. Hou, J. Lee, and H. Manouzi, “Finite element approximations of stochastic optimal control problems constrained by stochastic elliptic PDEs,” J Math Anal Appl, vol. 384, no. 1, pp. 87–103, Dec. 2011, doi: 10.1016/J.JMAA.2010.07.036.
[41] M. Wang and L. Chen, “Multigrid methods for the Stokes equations using distributive gauss-seidel relaxations based on the least squares commutator,” J Sci Comput, vol. 56, no. 2, pp. 409–431, doi: 10.1007/S10915-013-9684-1.
[42] M. M. Butt, “Multigrid Method for Optimal Control Problem Constrained by Stochastic Stokes Equations with Noise,” Mathematics 2021, Vol. 9, Page 738, vol. 9, no. 7, p. 738, Mar. 2021, doi: 10.3390/MATH9070738.
[43] I. Babuška, R. Temponet, and G. E. Zouraris, “Galerkin finite element approximations of stochastic elliptic partial differential equations,” SIAM J Numer Anal, vol. 42, no. 2, pp. 800–825, 2004, doi: 10.1137/S0036142902418680.
[44] W. Zulehner, “Nonstandard norms and robust estimates for saddle point problems,” SIAM Journal on Matrix Analysis and Applications, vol. 32, no. 2, pp. 536–560, 2011, doi: 10.1137/100814767.
[45] S. Takacs, “A robust all-at-once multigrid method for the Stokes control problem,” Numer Math (Heidelb), vol. 130, no. 3, pp. 517–540, Jul. 2015, doi: 10.1007/S00211-014-0674-5.
[46] Doi: 10.1016/J.APNUM.2018.03.002.